P H Y S I C A L   R E V I E W   L E T T E R S

Study of X-Ray Emission Enhancement via a High-Contrast Femtosecond Laser Interacting with a Solid Foil

L. M. Chen,[1,2] M. Kando,[1] M. H. Xu,[2] Y. T. Li,[2] J. Koga,[1] M. Chen,[2] H. Xu,[2] X. H. Yuan,[2] Q. L. Dong,[2] Z. M. Sheng,[2,3]
S. V. Bulanov,[1,*] Y. Kato,[1] J. Zhang,[2,3] and T. Tajima[1]

[1]*Advanced Photon Research Center, Kansai Photon Science Institute, JAEA, Kyoto 619-0215, Japan*
[2]*Beijing National Laboratory of Condensed Matter Physics, Institute of Physics, CAS, Beijing 100080, China*
[3]*Department of Physics, Shanghai Jiao Tong University, Shanghai 200240, China*
(Received 6 October 2006; published 30 January 2008)

We observed the increase of the conversion efficiency from laser energy to $K\alpha$ x-ray energy (η_K) produced by a 60 fs frequency doubled high-contrast laser pulse focused on a Cu foil, compared to the case of the fundamental laser pulse. η_K shows a strong dependence on the nonlinearly modified rising edge of the laser pulse. It reaches a maximum for a 100 fs negatively modified pulse. The hot electron efficient heating leads to the enhancement of η_K. This demonstrates that high-contrast lasers are an effective tool for optimizing η_K, via increasing the hot electrons by vacuum heating.

The availability of intense femtosecond (fs) lasers [1] makes new laser-solid interaction regimes. Hot electrons, generated via collective mechanisms such as resonant absorption (RA) [2] or vacuum heating (VH) [3], penetrate into the solid target and produce hard x ray via K-shell ionization and bremsstrahlung [4]. This kind of intense and ultrafast hard x-ray source has a number of interesting applications for medical imaging [5].

Control and optimization of the above mentioned hard x-ray emission relies on specifying the laser energy absorption and hot electron generation. Several groups have studied x-ray generation using subpicosecond laser systems [6–13]. Hundreds of fs laser pulses were produced by gas or glass laser systems [6,7]. The plasma density profile steepened due to the ponderomotive force [14]. As a result, optimal conditions for RA were realized [6]. RA was the main heating mechanism in this regime. Recently, it has been shown that using shorter laser pulses, with durations less than 100 fs, new x-ray emission processes are required in order to explain the observed phenomenon. Eder *et al.* observed a maximum in $K\alpha$ emission where the target was placed away from the best focus position [8]. This was qualitatively explained by the reabsorption of photons produced inside the target at high electron temperature. Based on the optimal scale length for RA, Reich *et al.* [9] found a scaling law for the optimal laser intensity dependence and predicted a reduction of the hard x-ray yield for high laser intensity. Zhidkov *et al.* [10] demonstrated large scale plasma density profile formation with $L = [(1/n) \times (dn/dx)]^{-1} = 2.5\lambda$ due to the amplified spontaneous emission. A decrease of the laser energy absorption for shorter pulse duration was observed. This phenomenon has also been proved in experiment [11] via the RA process. The above results show a limitation on the hard x-ray emission with increasing laser intensity for tens of fs laser pulse duration when low contrast leads to preplasma formation and to the RA mechanism.

In this Letter, we show that the limitation on the hard x-ray emission enhancement can be overcome by using high-contrast relativistic fs laser pulses. In this regime the "vacuum heating" is the main mechanism for the hot electron generation. It does not saturate with the laser intensity and results in enhancement of the x-ray emission. We control and optimize the yield of the x-ray emission via generating positively or negatively modified laser pulses. The Cu η_K reaches a maximum, 4×10^{-4}, for 100 fs negatively modified pulse irradiation.

The experiment is performed with the XL-II laser system at the Institute of Physics in China. The laser delivers a maximum energy of >300 mJ after compression with a pulse duration of 60 fs. The prepulse from 8 ns before the main pulse is better than 1×10^5. The laser contrast for the picosecond pedestal obtained using a third-order fs autocorrelator is 1×10^4 (see the inset of Fig. 1). A type I potassium dideuterium phosphate (KDP) frequency doubling crystal (1 mm thick) is used to get the 400 nm second harmonic pulse. The double-frequency conversion efficiency of the KDP crystal is about 40% at 200 GW/cm². The infrared light is rejected by passing the beam over 4 dielectric coated mirrors. This increases the pulse contrast compared to the picosecond pedestal $>10^8$ and $>10^{10}$ in the nanosecond time window. The p-polarized laser pulse is obliquely incident on a 5 μm thick Cu foil at 45° by an $f/3.5$ parabola mirror with a focal spot diameter of 10 μm (FWHM) and an average intensity of 1×10^{18} W/cm². By changing the interaction geometry, p- or s-polarized light could be used. The determination of the η_K is made with a single photon counting x-ray CCD camera as a spectrometer. An electron spectrometer is used to detect the electron spectrum [12]. An imaging plate is used for the electron angular distribution measurement. A knife edge is introduced to determine the source size. The FWHM of the source size is $\sim$10 μm, implying no evident plasma expansion.
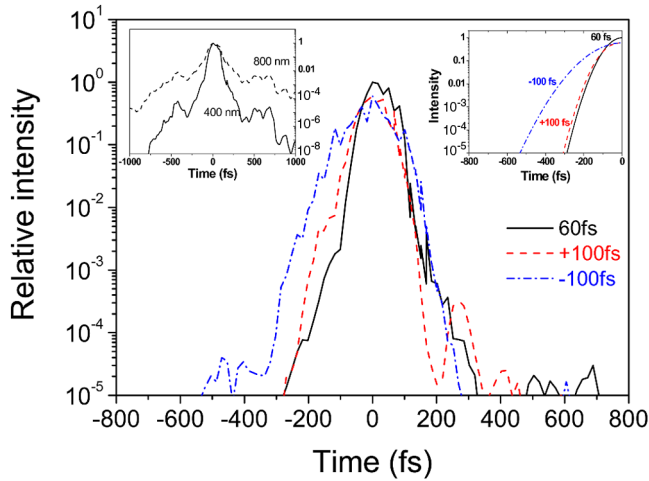
FIG. 1 (color online). Temporal pulse shape for the high-contrast 400 nm laser for 60 fs (solid line), 100 fs positively modified (dashed line), and 100 fs negatively modified (dash-dotted line), respectively. The left-hand inset shows the temporal profile for the low-contrast 800 nm pulse (dashed line) and the high-contrast 400 nm pulse (solid line). The 400 nm pulse profile is estimated from $I_{(400)} \sim I_{(800)}^2$. The right-hand inset shows the leading edge of the corresponding three curves of the temporal profile for a 400 nm laser fitted by a modified Gaussian form described in the text, with the modifying parameter $b = 0.5$.

The pulse duration is increased by detuning the compressor gratings, but then the uncompensated linear or B-integral phase reduces the pulse contrast. We were able to vary the laser pulse duration from 60 fs up to 2 ps by changing the distance between the gratings at constant laser energy. Increasing (decreasing) distance causes incomplete compensation of the accumulated phase nonlinearities resulting in negatively (positively) chirped pulses having a gentle (steep) rise time [13], as shown in Fig. 1 and the right-hand inset. A modified Gaussian is used to fit the temporal intensity profile of the modified laser pulse with the formula $I(t) = I_0 \exp\{[-t^2/(2\tau^2)]/[1 + bt/(t^2 + \tau^2)^{1/2}]\}$, where τ is the pulse duration and b is the modifying parameter [13], as the right-hand inset of Fig. 1 shows. The calculated Gaussian shapes fit reasonably to the measurement on the rising edge, which leads to the laser-plasma modulation. For a sample pulse, starting from the relative intensity $\sim 10^{-5}$, when the plasma begins to expand, to the intensity $\sim 10^{-1}$ before the pulse peak arrives, the rising times are 400, 200, and 200 fs for a laser with a pulse duration of 100 fs negatively modified, 100 fs positively modified, and 60 fs, respectively. This shows that positive 100 fs pulses have almost the same rising edge as the 60 fs laser pulse, whereas the negative pulse has double the expansion period and integrated energy within the rising edge. The development of the preplasma for the high-contrast laser is calculated using the hydrodynamic code HYADES [15]. The prevailing preplasma scale length (L/λ) is estimated as consisting of a density profile described by a Riemann solution of the hydrodynamic flow

equation $n(z) = n_0[1 - z/4L(t)]^3$ [16] for adiabatic expansion, and surface expansion velocity $4dL/dt = [2/(\gamma - 1)](ZkT_e/m_i)^{1/2} \sim 1.4 \times 10^7$ cm/s with $KT_e \sim 100$ eV. L/λ is 0.1, 0.05, and 0.05 corresponding to the 100 fs negatively modified, 100 fs positively modified, and 60 fs pulses, respectively; see the inset of Fig. 2(b). To correctly interpret the data, it is crucial to establish the proper compressor zero which corresponds to the shortest pulse duration. A KDP crystal is used for this purpose because the KDP energy conversion efficiency will decrease with increasing the pulse duration or introducing undesirable frequency chirp in the 800 nm pulses if the grating is not in the proper position. In our experiment, the KDP conversion efficiency is a maximum at the compressor grating zero position which we defined, demonstrating the shortest pulse duration.
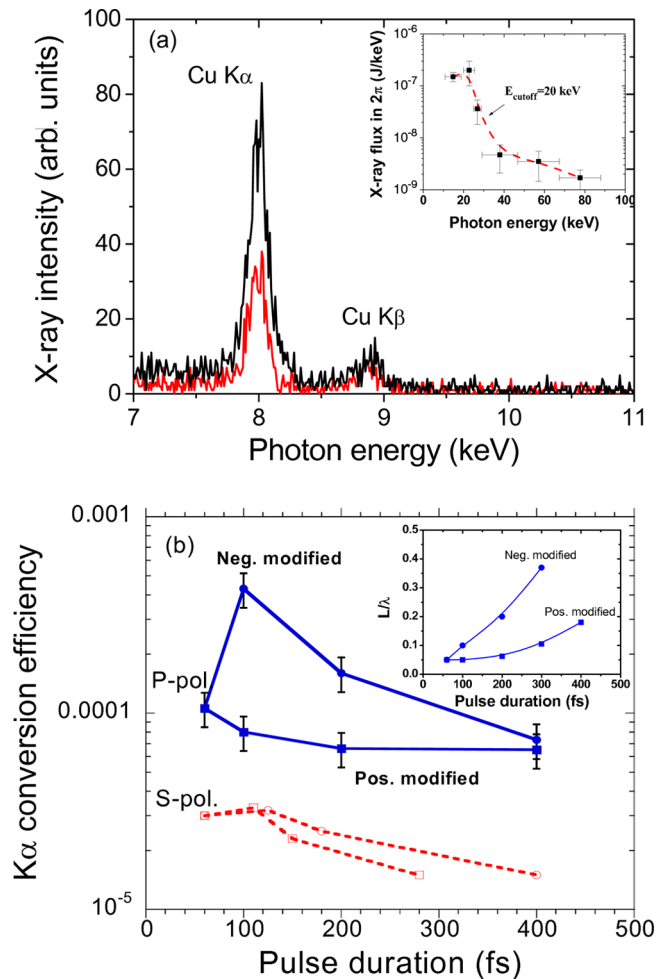

FIG. 2 (color online). (a) Cu hard x-ray spectra produced by 800 nm [gray (red) line] and 400 nm (black line) laser pulses at 1×10^{18} W/cm^2. The inset shows the continuous part of the spectrum. (b) Cu η_K as a function of laser pulse width with negatively modified (solid circle) and positively modified (solid square) for a p-polarized 400 nm laser, and also negatively modified (open circle) and positively modified (open square) for an s-polarized 400 nm laser. The inset shows the corresponding plasma scale length (L/λ) before the pulse peak arrives.

Figure 2(a) shows the spectra measured from a Cu foil target with the following parameters: 60 fs, 100 mJ, 1×10^{18} W/cm^2 at 800 nm and 400 nm wavelength with a p-polarized laser. We observe that the $K\alpha$ yield at 400 nm is 2 times higher than at 800 nm. The Cu η_K in 2π steradians reaches $\sim 1 \times 10^{-4}$. It should be noted however that the continuous part of x-ray spectrum is not distributed in a Maxwellian, and an evident energy cutoff ($E \sim$ 20 keV) exists as shown in the inset of Fig. 2(a). In order to optimize Cu η_K, we introduce a slightly long pulse duration with a nonlinearly modified pulse shape. Figure 2(b) shows Cu η_K as a function of the 400 nm laser pulse duration for negative and positive modification. It shows Cu η_K with the negative 100 fs pulse duration is dramatically improved, reaches a maximum of 4×10^{-4}, and is almost 5 times greater than the case of the positive pulse. However, for s-polarized laser incidence, Cu η_K is 3 times lower and does not show an evident pulse chirp dependence. It simply decreases with increasing laser pulse duration.

A higher η_K for the 400 nm laser pulse corresponds to a higher laser energy absorption with hot electron generation. If we consider that RA is the main mechanism, a 800 nm laser pulse should be more effective than a 400 nm one because the latter has a much weaker pedestal which induces a smaller L ($<0.1\lambda$) which is far away from the optimal scale length for RA [2]. However, our measurement does not agree with this assumption. Simulation shows VH dominates RA for a steep density gradient [3,17]. Under our laser conditions with intensity 1×10^{18} W/cm^2, $L = 0.05\lambda$. This agrees with the necessary condition to stimulate VH: electron quiver amplitude $X_{osc} \gtrsim L$. Other important evidence is the cutoff energy we detected, i.e., 20 keV, which rationally fits with the scaling law of VH: electron quiver energy $E_q = eE_L X_{osc} \sim 15$ keV in which E_L is the laser electrical field. This cutoff energy is lower than RA heated electrons with energy $E = eE_L L \sim 100$ keV typically [9] for low-contrast laser irradiation ($L \gg X_{osc}$). Moreover, this cutoff energy is suitable for maximizing the Cu K-shell ionization cross section which peaks at $E_e/E_{K\alpha} \sim 2-3$ [18] and producing $K\alpha$ photons just on the target surface which cannot be reabsorbed. The x-ray emission size (~ 10 μm) confirmed this energy. It is much smaller than for the 800 nm laser pulse case (>80 μm) [12]. Therefore, we conclude that VH is probably stimulated and may be the main absorption mechanism in the experiment.

Simulations using a 1D fully electromagnetic LPIC++ code have been performed, where an electromagnetic wave is launched obliquely (45°) onto an overdense plasma. We used the simulation parameters $a_0 = 0.33$, $\tau = 30$, $n_e/n_c = 20$, $T_e = 100$ eV, $T_e/T_i = 3 \sim 5$, and mass ratio $m_p/m_e = 1836$. The initial scale length $L/\lambda = 0.05$. Figure 3(b) shows the electric field at the target surface with a polarity which changes periodically, reflecting the "pull-push" procedure in each laser half period
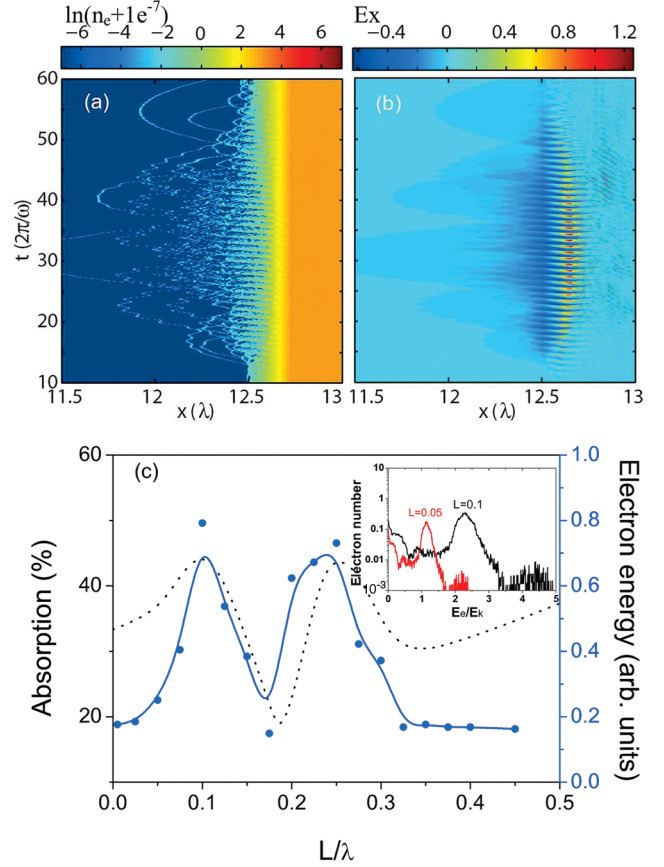

FIG. 3 (color). Temporal evolution of the electron density (a) and the longitudinal electric field E_x (in the boosted frame showing the pure electrostatic component) (b), where the initial density scale length $L = 0.05\lambda$ and the critical surface starts from $x = 12.55\lambda$. (c) Absorption rate (dotted line) and hot electron energy (solid line) as a function of L. The inset shows the electron spectra in the case of $L/\lambda = 0.05$ (red line) and 0.1 (black line).

[3,17]. A group of electrons is pulled out into vacuum at each optical cycle and returns to the target surface as shown in the temporal dependence of the electron density in Fig. 3(a). We note that the ion displacement is negligible during the laser-plasma interaction. All these phenomena demonstrate the stimulation of VH. Figure 3(c) shows that the energy absorption depends on the plasma density gradient at $\Delta t = 30$. There are 2 absorption peaks located at short scale with lengths $L/\lambda = 0.1$ and 0.25. According to the optimal scale length, the second peak corresponds to RA [2]. The first peak ($L/\lambda = 0.1$) results from VH; see Ref. [17]. The curve shows the stimulation of VH critically depends on L. This is a key character for VH which contributes to the emission enhancement and pulse shape dependence of the x rays. With a slight surface expansion of the scale length, the optical field would pull more electrons into vacuum and thus be more strongly absorbed [17,19], as long as L does not significantly exceed X_{osc}. In our experiments, the comparable larger pulse pedestal will lead to plasma expansion if we tune the pulse negatively
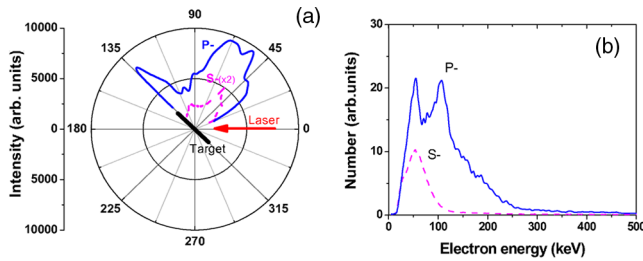
FIG. 4 (color online). Hot electron detection for *p*- and *s*-polarized 400 nm laser irradiation with a pulse duration of 60 fs. Angular distribution of the outgoing hot electrons observed (a) in the case of *p*-polarized (solid line) and *s*-polarized laser (dashed line) irradiation. (b) Hot electron spectrum observed at 125° for *p*-polarized (solid line) and *s*-polarized laser (dashed line) irradiation.

and match the optimal plasma gradient ($L/\lambda \sim 0.1$) for VH when the pulse width is 100 fs, resulting in the maximization of η_K. A positively modified pulse with the same pulse width had a shorter pedestal with a smaller ($\sim 40\%$) integrated energy in the pedestal; see Fig. 1. In this case, the stimulation of VH is not as efficient as the negatively modified case. The inset in Fig. 2(b) shows the optimal scale length is achieved for the negative 100 fs pulse, while for the positive pulse a much longer pulse duration (300 fs) is necessary with a pulse intensity too weak to effectively heat electrons for $K\alpha$ photon generation. In addition, the integrated hot electron energy shows a similar dependence on L/λ, as shown in Fig. 3(c) and its inset, the integrated hot electron energy in $L/\lambda = 0.1$ is 3 times stronger than the case of $L/\lambda = 0.05$. This qualitatively explains the x-ray emission dependence with a different laser pulse rising edge. We need to mention that this hard x-ray laser pulse shape dependence has not been observed in low-contrast, 800 nm laser irradiation. We also note Riley *et al.* used a plastic coating method to control preplasmas [20].

Hot electrons generated by an intense laser field are responsible for producing x rays as they interact with a solid target. The character of the outgoing electrons reveals important information. As Fig. 4(a) shows, the outgoing fast electron is concentrated along the target normal and specular reflection direction for the incident *s*-polarized laser. For *p*-polarized laser irradiation, the vacuum heated electron emission is much stronger, by a factor of 4–5, and shows broad emission close to the target normal. This is also a character of VH and an additional experimental verification. We also note an electron jet along the target direction (also discussed in Ref. [21]) is represented by fast surface electrons. Moreover, the fast electron spectrum for surface emission, seen in Fig. 4(b), shows a *peaked* structure. There is an individual second peak with energy ~ 110 keV for *p*-polarized laser irradiation. This means a group of quasimonoenergetic electrons is observed for the first time in surface emission. A detailed explanation is beyond the scope of this Letter.

In summary, Cu η_K produced by a high-contrast laser pulse at 400 nm with intensity 1×10^{18} W/cm^2 reaches 4×10^{-4}, due to the efficient generation of hot electrons which shows a "peaked" spectrum. Tunable control of the hard x-ray emission is successful via controlling pulse duration and modifying the pulse rising edge. This implies an effective method for x-ray enhancement in the fs-plasma regime: resonant absorption may be noneffective in fs laser-dense plasma interactions [12], whereas a high-contrast laser is more efficient for hard x-ray generation via vacuum heating.

*Also at: A. M. Prokhorov Institute of General Physics of Russian Academy of Sciences, Moscow, Russia.
[1] D. Strickland and G. Mourou, Opt. Commun. **56**, 219 (1985).
[2] W. L. Kruer, *The Physics of Laser Plasma Interactions* (Addison-Wesley, New York, 1988); V. L. Ginzburg, *The Propagation of Electromagnetic Wave in Plasmas* (Pergamon, New York, 1970); S. V. Bulanov *et al.*, Phys. Rep. **186**, 1 (1990).
[3] F. Brunel, Phys. Rev. Lett. **59**, 52 (1987).
[4] H. Chen *et al.*, Phys. Rev. Lett. **70**, 3431 (1993).
[5] A. Krol *et al.*, Med. Phys. **24**, 725 (1997).
[6] B. Soom *et al.*, J. Appl. Phys. **74**, 5372 (1993); S. Bastiani *et al.*, Phys. Rev. E **56**, 7179 (1997); Z. Jiang *et al.*, Phys. Plasmas **2**, 1702 (1995); E. Andersson *et al.*, J. Appl. Phys. **90**, 3048 (2001); M. Schnurer *et al.*, J. Appl. Phys. **80**, 5604 (1996).
[7] U. Teubner *et al.*, Phys. Rev. Lett. **70**, 794 (1993).
[8] D. C. Eder *et al.*, Appl. Phys. B **70**, 211 (2000).
[9] Ch. Reich *et al.*, Phys. Rev. Lett. **84**, 4846 (2000); D. Salzmann *et al.*, Phys. Rev. E **65**, 036402 (2002).
[10] A. Zhidkov *et al.*, Phys. Rev. E **62**, 7232 (2000).
[11] M. Schnurer *et al.*, Phys. Rev. E **61**, 4394 (2000).
[12] L. M. Chen *et al.*, Phys. Plasmas **11**, 4439 (2004).
[13] W. P. Leemans *et al.*, Phys. Rev. Lett. **89**, 174802 (2002); U. Andiel *et al.*, Appl. Phys. Lett. **80**, 198 (2002); T. Guo *et al.*, Rev. Sci. Instrum. **72**, 41 (2001).
[14] D. T. Attwood *et al.*, Phys. Rev. Lett. **40**, 184 (1978).
[15] J. T. Larsen and S. M. Lane, J. Quant. Spectrosc. Radiat. Transfer **51**, 179 (1994).
[16] Y. B. Zeldovich and Y. P. Raizer, *Physics of Shock Waves and High-Temperature Hydrodynamic Phenomena* (Academic, New York, 1966).
[17] P. Gibbon and A. R. Bell, Phys. Rev. Lett. **68**, 1535 (1992).
[18] C. Hombourger, J. Phys. B **31**, 3693 (1998).
[19] M. K. Grimes *et al.*, Phys. Rev. Lett. **82**, 4010 (1999).
[20] D. Riley *et al.*, Phys. Rev. E **71**, 016406 (2005); F. Y. Khattak *et al.*, Phys. Rev. E **74**, 027401 (2006).
[21] Y. T. Li *et al.*, Phys. Rev. Lett. **96**, 165003 (2006); H. Habara *et al.*, Phys. Rev. Lett. **97**, 095004 (2006); Z. Li *et al.*, Phys. Plasmas **13**, 043104 (2006).